Atmospheric
Chemistry
and Physics
Discussions

Open Access

Analysis of extinction properties as a function of relative humidity using a κ-EC-Mie model in Nanjing

Zefeng. Zhang[1], Yan. Shen[1], Yanwei. Li[1], Bin. Zhu[1], Xingna. Yu[1]

[1]Collaborative Innovation Center on Forecast and Evaluation of Meteorological Disasters, Key
Laboratory for Aerosol-Cloud-Precipitation of China Meteorological Administration, Nanjing
University of Information Science & Technology, Nanjing, 210044, China
Correspondence to: Y. L Li (liyw@nuist.edu.cn)

Abstract The relationship between relative humidity (RH) and extinction properties is of widespread

concern. In this study, a hygroscopic parameter (κ) and the volume fraction of elemental carbon (EC)

were used to characterize the chemical characteristics of particles, and a core-shell model was built based

on these characteristics. The size distribution, chemical compositions and RH were measured in Nanjing

from 15/10/2013 to 13/11/2013. The extinction coefficients of particles were fitted with the BHCOAT

program, and the values correlated well with the measured values (R^2=0.81), which suggested that the

core-shell model was reasonable. The results show that more than 83% of the extinction in Nanjing was

due to particles in the 0.2-1.0μm size range. Under dry conditions, the higher mass fraction of particles in

the 0.2-1.0μm size range caused the higher volume extinction coefficient. An increase in RH led to a

significant increase in the extinction coefficient, although the increases differed among the different size

segments. The corresponding functions are given in this study. For λ=550 nm, the extinction

contributions of the 0.01-0.2μm, 0.2-0.5μm, and 1.0-2.0μm size ranges increased significantly with the

increase in RH, whereas the extinction contributions of the 0.5-1.0μm and 2.0-10.0μm size ranges

decreased slightly.

1 Introduction

The degradation of visibility is likely the most readily perceived impact of aerosol pollution and has been

used as a visual indicator of ambient air quality (Watson, 2002). Visibility throughout the world has

generally decreased in recent decades, especially in Asia. In China, horizontal visibility has significantly

decreased since 1980 (Che et al., 2007; Qian and Giorgi, 2000; Qian et al., 2007; Streets et al., 2008; Fu

et al., 2013). For example, in Guangzhou, one of the largest cities in the Pearl River Delta (PRD) , low

visibility occurs 150 days•year^{-1} (Deng et al., 2008). In the Beijing-Tianjin-Hebei region, the annual

Atmospheric
Chemistry
and Physics
Discussions

Open Access

EGU

average number of continuous haze events has increased, accounting for more than half of the total haze

days in a year(Zhang et al., 2015). In the Yangtze River Delta (YRD) region, visibility has decreased at

the rate of 2.41 km•decade^{-1}(Gao et al., 2011). Visibility degradation mainly caused by the increase of

particle concentration and easily lead to a variety of health problems (such as cardiovascular disease,

5   respiratory system diseases, etc.) and traffic accidents increasing, which has a serious impact on human

health and activities.(Tie et al., 2009; Wu et al., 2005; Chang et al., 2009). As a result, visibility problems

have received unprecedented attention in recent years.

Under dry conditions, the extinction of particles is the main factor affecting visibility (Covert et al., 1972;

Deng et al., 2008; Watson, 2002). The particle size distribution, chemical composition and relative

10   refractive index determined by the chemical composition are the important parameters that affect the

optical properties of the particles(Day et al., 2000; Ma et al., 2012; Cheng et al., 2008a; Wen and Yeh,

2010). However, many of the aerosol components are hygroscopic and take up water as a function of the

relative humidity (RH) (Clarke et al., 2004; Covert et al., 1972). When the RH is high, the hygroscopic

growth of the particles will lead to an increase in size and a decrease in the refractive index, which have

15   significant effects on the extinction properties(Cheng et al., 2008b; Covert et al., 1972; Stock et al., 2011).

Furthermore, the physicochemical properties of aerosols lead to variable hygroscopic growth, and the

extinction associated with different particles is significantly different under the same RH. Overall,

visibility will decrease when the RH increases (Charlson, 1969; Covert et al., 1972; Stock et al., 2011;

Day and Malm, 2001). Some studies show that extinction can increase by more than 100% when the RH

20   exceeds 70%-80% (Mcmurry, 2000; Zhang and Mcmurry, 1992; Tang, 1996). Therefore, the study of the

effect of RH on the extinction coefficient is very important.

Interest in the relationship between aerosol composition, RH and visibility dates back to at least to the

studies of Wright (1940) on the atmospheric opacity over Valentia, Ireland (Wright, 1940). Currently, we

can calculate the extinction coefficient accurately based on the Mie theory (Bohren and Huffman, 2008)

25   if we have information on the physicochemical properties of all the particles. However, atmospheric

particles consist of a complicated mixture of various chemical compositions, and it is very difficult to

obtain complete data on the physicochemical properties of all particles. In field observations, a fitting

formula is often used to assess the contribution of RH, thought this method cannot reflect the differences

in physicochemical properties of particles and fitting curves are different at different sites(Chen et al.,

30   2010; Yu et al., 2015). Another method is based on chemical composition and involves calculation of the

extinction coefficient using an empirical formula for different RH values. Of course, this method   leads
to great uncertainty. Therefore, we must establish a model that has few variables and for which each
variable can be obtained based on conventional observations. The three-component model is an
important hypothesis(Cheng et al., 2006). The first component is elemental carbon (EC), which is the

5   light-absorbing component. The real and imaginary parts of EC are extremely high, and a typical value is
1.8- 0.54i (Lee and Tien, 1981; Redemann et al., 2000). Water is the second component, which   only
scatters the incident radiation with the lowest refractive index of 1.33-0.0i (Levoni et al., 1997). Aside
from EC and water, the rest of the aerosol components primarily only scatter light with very similar
refractive indexes, with a real part of approximately 1.53 and an imaginary part of nearly zero. This

10   component is called the non-light-absorbing component (Lin et al., 2013; Tang, 1996; Wex et al., 2002).
Wex's study showed that the simplification is reasonable (2002). He found that, under dry conditions,
there was no statistically significant effect on the deviation between the measured and calculated
scattering coefficients when varying the mass fractions of the nearly pure light-scattering compositions
within their general concentration levels. Thus, if we know the volume fraction of EC, we can better

15   describe the extinction properties of the particles. . Particles show hygroscopic growth as the RH
increases. Petters and Kreidenweis (2007) proposed a simple hygroscopic parameter, κ, that can be used
to calculate the hygroscopic growth factor (GF) at different levels of RH. κ can be considered a function
of the chemical composition and volume fraction of the non-light-absorbing component because the
hygroscopic growth of EC is poor. Supposing that non-light-absorbing material is uniformly mixed with

20   water after hygroscopic growth, we can determine the changes in volume of both the real part and
imaginary parts, then calculate the extinction coefficient of particles (Chen et al., 2012).Therefore, we
can calculate the extinction properties of particles accurately at different levels of RH based on the Mie
theory according to the three-component model, as long as we obtain the volume fraction of EC, the
hygroscopic parameter (κ) and the hypothesized mixed mode of the aerosols.

25   In this study, the volume fraction of EC and the hygroscopic parameter (κ) were obtained using film
sampling. Film sampling was used to analyze the chemical composition of particles that were most
common and oldest, with abundant observational data. Verifying the reasonability of the κ-EC-Mie
model will help demonstrate its practical applicability. In this study, the volume fraction of EC was
obtained from the film sampling conducted using an   Anderson instrument in Nanjing and κ was

30   calculated according to the ZSR rule(Petters and Kreidenweis, 2007). The extinction coefficient

Atmospheric
Chemistry
and Physics
Discussions

calculated by the above method had a good relationship with the visibility, which verified the reasonableness of our method. Based on this result, we further explored the growth curve of the extinction coefficient as the RH increased and the variety of extinction contributions provided by different particle sizes.

2 Experiment and methods

2.1 Measurement location and sampling

The sampling site was on the roof of a twelve-story building at the Nanjing University of Information Science and Technology in the Pukou District of Nanjing (32.207 °N; 118.717 °E), 40 m above the ground. Visibility and meteorological parameters were obtained from the detection base near the sampling site at a distance of less than 1.5 km. The sampling period was from 15/10/2013 to 13/11/2013. The periods of instrumental observation are shown in Fig. 1, and the missing data were due to power failure. Moreover, because the measurement error is high at high RH values, we excluded the data with an RH >90% and visibility <1 km.

Fig. 1 Missing data from instruments during the observation period

2.2 Instruments and data analysis

2.2.1 Instruments

A wide-range particle spectrometer (WPS; MSP Corporation model 1000XP) is a recently introduced commercial instrument with the unique ability to measure the size distributions of aerosols with diameters from 0.01 to 10μm (Liu, 2010). The WPS combines the principles of differential mobility analysis (DMA), condensation particle counting (CPC) and laser light scattering (LPS). DMA and CPC are used to measure particles in the size range of 10-500 nm, and LPS is used to measure particles in the range of 0.35-10μm. One complete scan of the entire size range with a 3 s scanning period for each channel takes approximately 5 min, and a detailed description was provided previously(An et al., 2015; Kang et al., 2013).

Anderson is a nine-stage impact sampler that is produced by the Thermo Electron Corporation (USA). It was used to collect aerosol samples. The sampling flow rate is 28.3 L•min^{-1}. The size distributions were ≤0.43μm, 0.43-0.65μm, 0.65-1.1μm, 1.1-2.1μm, 2.1-3.3μm, 3.3-4.7μm, 4.7-5.8μm, 5.8-9.0μm

Atmospheric
Chemistry
and Physics
Discussions

and >9.0μm. We used cellulose filters for ionic species and quartz filters for EC and OC(organic carbon). For further discussion of the processing steps, please refer to Zou et al.(2014).

Water-soluble ions were measured with a chromatograph (850 professional IC). Na^+, NH_4^+, Ca^{2+}, Mg^{2+}, K^+, F^-, Cl^-, NO_2^-, NO_3^- and SO_4^{2-} were analyzed in this study, and a detailed description was provided

5   previously (An et al., 2015).

The EC and OC were determined with a thermal/optical carbon analyzer (Model 2001A, DRI). The principle instrument and processing method have previously been described in detail (Miao et al., 2015; Zou et al., 2014).

$PM_{2.5}$ was detected with a β-ray particulate continuous monitor (Thermo Fisher). And the working

10   principles was that measuring particles' mass concentration through β-ray attenuation. Visibility data were collected with a CJY-1 visibility meter(CAMA Measurement & Control Equipments Co., Ltd). The visibility meter was used to measure scattering coefficient of particles and it's light source wavelength was 940nm. A detailed description of these two instruments was provided previously (Yu et al., 2015).

15   **2.2.2 Calculation of the hygroscopic parameter (κ)**

κ can be calculated according to many methods (Liu et al., 2014; Miao et al., 2015; Petters and Kreidenweis, 2007). In this study, κ was calculated with the ZSR rule(Petters and Kreidenweis, 2007)according to the chemical composition of the particles. For an inorganic component, we considered a system containing H^+, NH_4^+, HSO_4^-, SO_4^{2-}, and NO_3^{2-}. Gysel et al. (2007) used the ion

20   pairing method, and his method is more precise than the ADDEM model (Δ g/g<2%) (Topping et al., 2005). For each species, the molecular weight, κ and density are described in detail in Table 1 (Gysel et al., 2007; Kreidenweis et al., 2008; Petters and Kreidenweis, 2008; Topping et al., 2005). Moreover, we considered the effect of water-soluble organic components (WSOC) on hygroscopic growth and assumed $\kappa_{org}=0.1$ (Jimenez et al., 2009; King et al., 2010).

25   We can obtain the mass of each pure species according to the pairing method. Supposing a dry particle's density is 1.7 g•cm^{-3} (Wehner et al., 2008), we can calculate the volume of the dry particle. Aside from the WSOC and the four types of inorganic components in Table 1, we assumed that other components do not contribute to the hygroscopic properties of the aerosols. According to the ZSR rule, κ is given by Eq. (1):

Atmospheric
Chemistry
and Physics
Discussions

$$\kappa = \sum_{i=1}^{N} \kappa_i \frac{V_{i,dry}}{V_{tol,dry}}$$

(1)

Table 1 Properties of each pure material

2.2.3 Calculation of the hygroscopic growth factor (GF)

5 The hygroscopic growth behavior of particles can be described by the theory of Köhler (1936). The

theory of Köhler considered the Kelvin effect and Raoult effect and established a relationship among the

saturation ratio S (at sub-saturation, S is equivalent to RH), diameter and solute properties. Introducing

the hygroscopic parameter κ (Petters and Kreidenweis, 2007), the hygroscopic growth factor (GF) is

determined as follows in Eq. (2):

10 $$GF = \left(1 + \frac{\kappa \cdot S}{\exp\left(\frac{4\sigma_{s/\alpha} M_w}{RT\rho_w}\right) - S}\right)^{\frac{1}{3}}$$

(2)

where M_w is the molar mass of water, R is an ideal gas constant, ρ_w is the density of water, T=20 °C, and

$\sigma_{s/\alpha}$ is assumed to be the surface tension coefficient between water and air (when T=20°C, $\sigma_{s/\alpha}$=0.0728 N

m^{-1}).

15 ### 3 Results and discussion

3.1 Aerosol properties and visibility during the measurement period

A time series of RH, visibility, extinction coefficient, and PM$_{2.5}$ during the observation period is shown

in Fig. 2. The extinction coefficient was calculated as 3.0/visibility (Seinfeld and Pandis, 2012). The

picture shows that the visibility has a strong negative correlation with PM$_{2.5}$ and RH (R=-0.67 and -0.62,

20 respectively). A time series of size distribution for dry particles is given by Fig. 3,We find that the

periods of high particles number concentration had a good consistent with periods of high PM$_{2.5}$ mass

concentration . Fig. 4 shows the time series of κ for different particle sizes. κ was calculated according to

the ZSR rule, which is described in detail in Section 2.2.2. Fig. 5 shows the time series of the volume

fraction of EC in different size segments, and the volume fraction of EC was calculated using data from

25 the Anderson instrument. Fig. 4 and Fig. 5show that κ and the volume fraction of EC changed over time,

but the degree of change in different size segments was larger than that at different times. The reason for

this difference may be that the particle size was closely related to the sources. Considering that the

Atmospheric
Chemistry
and Physics
Discussions

methods of film sampling and WPS differ significantly in time resolution, we made the following assumptions: 1) the chemical compositions of particles were unchanged for a given diameter segment of Anderson; 2) the chemical composition of particles remained unchanged over the course of a day.

Fig. 2 Time series of RH, visibility, extinction coefficient, and $PM_{2.5}$ during the observation period

5   Fig. 3 Time series of size distribution (dry particles) during the observation period

Fig. 4 Time series of κ for different sizes during the observation period

Fig. 5 Time series of the volume fraction of EC for different size segments during the observation period

3.2 Comparative analysis of the calculated and observed values of the aerosol extinction coefficient
10   by the core-shell model

Under dry conditions, the volume fraction of EC can describe the volume fraction of the light-absorbing component and κ can describe the hygroscopicity of the particle. We believe that these two parameters can be used to calculate the extinction coefficient of a single particle accurately at different RH levels. In the real atmosphere, even if the sizes of aerosol particles are the same, the physicochemical properties of

15   particles are significantly different. It is unrealistic to describe the physicochemical properties of the aerosols individually. Therefore, the internally mixed model, externally mixed model, and core-shell model are often used to describe the chemical composition of aerosol particles in practical studies (Lesins et al., 2002; Cheng et al., 2006; Hao et al., 2010). The calculation results of the core-shell model are usually between those of the internally mixed model and externally mixed model(Hao et al., 2010).

20   Therefore, the core-shell model was used in this study.

In this study, the core-shell model operates under the following assumptions: 1) particles of the same size have the same physicochemical properties, and particles are spherical; 2) under dry conditions, particles are composed of a light-absorbing component (EC, 1.8-0.54i) and a non-light-absorbing component (1.53-0i), and the EC is a spherical "core" that is always at the center of the particle; 3) GF as a function

25   of κ, the hygroscopic level of EC is poor, and the non-light-absorbing material is uniformly mixed with water after hygroscopic exposure.

According to the hypothesis of the core-shell model, we can calculate the extinction coefficient of the particles using Eq. (3). N was the number of size segments of the WPS (0.01-10 μm), with a value was 67. In this study, particles in the range of 0.5-10μm were measured by LPS. The term n represents the

30   number concentration of size segment N_i (i from 1 to 67), and r_i is the median radius corresponding to N_i.

Atmospheric
Chemistry
and Physics
Discussions

Q is an efficiency factor calculated with the BHCOAT program. The input/output parameters of Q and

the formulas are listed in Table 2. In Table 2, X is a scale parameter. D_0 is the diameter of a single particle

under dry conditions. λ is the incident light wavelength(λ=550 nm, 940 nm). The wavelength of light

source of the visibility meter was 940nm, and the calculated value of λ =940nm was used to contrast

5   with the observed value of the visibility meter. 550 nm is the most sensitive wavelength for the human

eye, and its calculated value was consistent with the human eye. GF is the hygroscopic growth factor,

which was calculated using Eq. (2). If RH=0, then GF=1. The complex refractive index was calculated

with the volume weighting method after the hygroscopic growth of the particle (Lesins et al., 2002).

$b_{ext} = \sum_{i=1}^{N} Q_{ext} \times \pi(r \times GF)_i^2 \times n(r_i)$

10   (3)

Table 2 Input/output parameters of the efficiency factor (Q)

Figure 6 shows the relative values of the calculated and observed values from the core-shell model.

When λ=940 nm, the time series of calculated and observed values were in good agreement (R^2=0.754),

which indicated that using the hygroscopic parameter (κ) and volume fraction of EC to characterize the

15   chemical characteristics of particles was reasonable. When λ=550 nm, the correlation coefficient of the

calculated and observed values (R^2=0.714) was slightly lower than when λ= 940 nm, mainly due to the

differences in the wavelength of the light source. Comparing the extinction values of 550 nm and 940 nm,

we found that the extinction coefficient at 550 nm was higher, mainly due to the differences in scale

parameters, which led to a Q that was larger when λ=550 nm. Because 550 nm is the most sensitive

20   wavelength for the human eye, the following section adopts 550 nm for discussion.

Fig. 6 Relationships among the calculated and observed values based on the core-shell model (λ=550 nm,

940 nm)

3.3 Contribution fraction of the extinction coefficient for different size segments under dry conditions

25   In the core-shell model, we defined GF=1 and then used Eq. (3) to calculate the extinction coefficients of

particles under dry conditions. We can calculate the extinction coefficients of particles in different size

segments with different median radii (r). In this study, particle size was divided into five segments:

0.01-0.2μm, 0.2-0.5μm, 0.5-1.0μm, 1.0-2.0μm, and 2.0-10.0μm. Fig. 7(a) shows the time series of the

extinction coefficients in different size segments under dry conditions, and Fig. 7(b) shows the

contribution fractions of the extinction coefficients in different size segments under dry conditions. Fig.

7(b) shows that the contribution fractions of the extinction coefficient in different size segments were

significantly different. On average, the 0.2-0.5 µm and 0.5-1.0 µm ranges together contributed more than

83% of the extinction coefficients, much higher than their PM_{10} mass fraction (45%). This result

5   suggests that, an increase in the proportion of particles in the 0.2-1.0 µm size range in PM_{10} will result in

an even greater increase in the extinction capacity relative to the unit mass of the particles. This result is

consistent with the results of Kang et al. (2013).

Fig. 7 Time series of extinction coefficients (a) and the contribution fractions of extinction coefficient (b)

in different size segments under dry conditions

10   Fig. 8 Time series of extinction coefficients (a) and the contribution fractions of extinction coefficient (b)

in different size segments at ambient relative humidity

3.4 Effects of relative humidity on the extinction coefficient

For ambient RH, we can calculate the extinction coefficients of particles in different size segments

using Eq. (3). Fig. 8(a) shows the time series of extinction coefficients in different size segments at

15   ambient RH, and Fig. 8(b) shows the contribution fractions of the extinction coefficient in different size

segments at ambient RH. Comparing Fig. 7 and Fig. 8, we found that the extinction coefficients in

different size segments at ambient RH were larger than for particles under dry conditions.

Simultaneously, the contribution fraction of the extinction coefficient in different size segments

underwent significant changes. Generally speaking, when particles were in the 0.01-0.2µm, 0.2-0.5µm

20   and 1.0-2.0µm size ranges, the contribution fraction of the extinction coefficients all increased,

especially for fine particles. When particles were in the 0.5-1.0µm and 2.0-10.0µm size ranges, the

contribution fraction of the extinction coefficients decreased.

The results shown in Fig. 8(a) were divided by those in Fig. 7(a) to produce the results in Fig. 9(a). The

y-axis represents growth multiples of the extinction coefficients compared to dry conditions. The x-axis

25   represents the variability of RH. There are five fitting curves in Fig. 9(a), representing different size

segments, and the correlation coefficient (R^2) of each fitting curve was more than 0.9. This result

suggests that, on different days, the changes in the extinction coefficients with the RH in the same size

segment were consistent. In addition, the extinction coefficient of particles in the 0.01-0.2µm size range

increased the fastest with the increased RH, followed by the extinction coefficients of particles in the

Atmospheric
Chemistry
and Physics
Discussions

0.2-0.5μm and 1.0-2.0μm size ranges. The extinction coefficients of particles in the 0.5-1.0μm and 2.0-10.0μm size ranges did not obviously increase with the increased RH. Because the average particle size distribution and chemical composition in each size segment are known, we can calculate the average contribution fraction of the extinction coefficients in each size segment with the increase in RH. The

5   calculation results are shown in Fig. 10, which illustrates that the extinction coefficient was primarily related to particles in the 0.2-0.5μm and 0.5-1.0μm size ranges. Generally speaking, an increase in RH will lead to an increase in the extinction coefficient, but the rate of increase in the extinction coefficient was significantly different in each size segment. With an increase in RH, the fractions of the extinction coefficients contributed by   the 0.01-0.2μm, 0.2-0.5μm, and 1.0-2.0μm size ranges increased

10   considerably, whereas the fractions of the extinction coefficient contributed by the 0.5-1.0μm and 2.0-10.0μm size ranges decreased slightly.

The impact of RH on particles was reflected in two aspects: the variability in diameter and the efficiency factor (Q). The growth of particles was determined by the hygroscopic parameter (κ). As κ increased, GF also increased. Fig. 4 shows the time series of κ for different particle sizes during the observations. The

15   particles in the 0.5-1.0μm range had the largest κ, which means that the variability in diameter cannot explain the lack of obvious increase in the extinction coefficients in the 0.5-1.0μm size range. To obtain Q following the influence of RH, we performed the following calculation. Firstly, we assumed that the RH had no effect on Q, which means that Q was equivalent to the value under dry conditions. Secondly, we calculated the extinction coefficient of particles in different size segments using Eq. (3)

20   (indicated by the letter b). Lastly, Fig. 8(a) was divided by b to produce Fig. 9(b), which represented the variation in Q with respect to RH. Fig. 9(b)shows that Q increased significantly in the 0.01-0.2μm, 0.2-0.5μm, and 1.0-2.0μm size ranges with the increase in RH and that Q declined slightly in the 0.5-1.0μm and 2.0-10.0μm size ranges at high RH values. The fitting curve and the calculated values are significantly different. For particles in the 0.01-0.2 μm, 0.2-0.5 μm, 0.5-1.0 μm and 1.0-2.0 μm size

25   ranges, the correlation coefficients are all high. Because λ=550 nm, the increase in the scale parameter in the 0.01-0.2μm, 0.2-0.5μm, and 1.0-2.0μm size ranges favors the increase in Q, whereas the increase of the scale parameter in the 0.5-1.0μm size range   leads to a decrease in Q. For particles in the 2.0-10.0 μm range, the correlation coefficient is very low. This finding suggested that the effect of the variation in the scale parameter on Q was significantly different on different days. In summary, variation in the scale

30   parameter leads to variation in Q, which is the main reason that growth multiples of the extinction

Atmospheric
Chemistry
and Physics
Discussions

coefficients vary at different RH levels.

Fig. 9 The effect of relative humidity on extinction

Fig. 10 Relationship between the contribution fraction of the extinction coefficient in different size

segments and relative humidity (RH)

5   **4 Conclusions**

In this study, a hygroscopic parameter (κ) and the volume fraction of elemental carbon (EC) were used to

characterize the chemical characteristics of particles and a core-shell model was built based on these

characteristics. In the core-shell model,   the real part and the imaginary part of the refractive index, the

scale parameters were both functions of RH. The extinction coefficients of particles fitted with the

10   BHCOAT program correlated well with the measured values (R^2=0.81), which suggested that using κ

and the volume fraction of EC to characterize the chemical characteristics of particles was reasonable.

In the core-shell model, when λ=550 nm, the contribution fractions of the extinction coefficient of

different size segments were significantly different. Under the dry condition, more than 83% of the

extinctions in Nanjing was contributed by particles in the 0.2-1.0μm size range, a much higher

15   percentage than their PM_{10} mass fraction(45%). This finding suggested that, for PM_{10}, an increase in the

mass proportion of particles in 0.2-1.0μm size range results in an even greater increase in the extinction

capacity.

With the increase in RH, the extinction capacity of particles will grow significantly. In this study, the

formula for the increase in extinction coefficients in different size segments is given. At given RH, the

20   growth rate of extinction coefficients differs significantly among different size segments. The growth

rates are related to κ, but the variation in the scale parameter leads to variations in Q, which is the main

reason that the growth multiples of the extinction coefficient differ at different RH values. With the

increase in RH, the extinction coefficient contribution fractions increase for particles in the 0.01-0.2μm,

0.2-0.5μm and 1.0-2.0μm size ranges but decrease for particles in the 0.5-1.0μm and 2.0-10.0μm ranges.

25   **References**

An, J., Wang, H., Shen, L., Zhu, B., Zou, J., Gao, J., and Kang, H.: Characteristics of new particle

formation events in Nanjing, China: Effect of water-soluble ions, Atmos. Environ., 108, 32-40,

Atmospheric
Chemistry
and Physics
Discussions

doi: 10.1016/j.atmosenv.2015.01.038, 2015.

Bohren, C. F., and Huffman, D. R.: Absorption and Scattering of Light by Small Particles, John Wiley & Sons, New York, 2008.

Chang, D., Song, Y., and Liu, B.: Visibility trends in six megacities in China 1973–2007, Atmos. Res., 94, 161-167, 2009.

Charlson, R. J.: Atmospheric visibility related to aerosol mass concentration: review, Environ. Sci. Technol., 3, 913-918, 1969.

Che, H., Zhang, X., Li, Y., Zhou, Z., and Qu, J. J.: Horizontal visibility trends in China 1981–2005, Geophys. Res. Lett., 34, L24706, doi: 10.1029/2007GL031450, 2007.

Chen, J., Zhao, C. S., Ma, N., Liu, P. F., Göbel, T., Hallbauer, E., Deng, Z. Z., Ran, L., Xu, W. Y., and Liang, Z.: A parameterization of low visibilities for hazy days in the North China Plain, Atmos. Chem. Phys., 12, 4935-4950, 2012.

Chen, Y., Zhao, D., Chai, F., Liang, G., Xue, Z., Wang, B., Liang, Y., Chen, Y., and Zhang, M.: Correlation between the atmospheric visibility and aerosol fine particles concertrations in Guangzhou and Beijing, China Environ. Sci., 7, 967-971, 2010.

Cheng, Y. F., Eichler, H., Wiedensohler, A., Heintzenberg, J., Zhang, Y. H., Hu, M., Herrmann, H., Zeng, L. M., Liu, S., and Gnauk, T.: Mixing state of elemental carbon and non‐light‐absorbing aerosol components derived from in situ particle optical properties at Xinken in Pearl River Delta of China, J. Geophys. Res. Atmos. (1984–2012), 111, 2006.

Cheng, Y. F., Heintzenberg, J., Wehner, B., Wu, Z. J., Su, H., Hu, M., and Mao, J. T.: Traffic restrictions in Beijing during the Sino-African Summit 2006: aerosol size distribution and visibility compared to long-term in situ observations, Atmos. Chem. Phys., 8, 7583-7594, 2008a.

Cheng, Y. F., Wiedensohler, A., Eichler, H., Su, H., Gnauk, T., Brüggemann, E., Herrmann, H., Heintzenberg, J., Slanina, J., and Tuch, T.: Aerosol optical properties and related chemical apportionment at Xinken in Pearl River Delta of China, Atmos. Environ., 42, 6351-6372, 2008b.

Clarke, A. D., Shinozuka, Y., Kapustin, V. N., Howell, S., Huebert, B., Doherty, S., Anderson, T., Covert, D., Anderson, J., and Hua, X.: Size distributions and mixtures of dust and black carbon aerosol in Asian outflow: Physiochemistry and optical properties, J. Geophys. Res. Atmos., 109, 839-856, 2004.

Atmospheric
Chemistry
and Physics
Discussions

Covert, D. S., Charlson, R. J., and Ahlquist, N. C.: A study of the relationship of chemical composition and humidity to light scattering by aerosols, J. Appl. Meteorol., 11, 968-976, 1972.

Day, D. E., Malm, W. C., and Kreidenweis, S. M.: Aerosol light scattering measurements as a function of relative humidity, J. Air Waste Manage. Assoc., 50, 710-716, 2000.

5   Day, D. E., and Malm, W. C.: Aerosol light scattering measurements as a function of relative humidity: a comparison between measurements made at three different sites, Atmos. Environ., 35, 5169-5176, 2001.

Deng, X., Tie, X., Wu, D., Zhou, X., Bi, X., Tan, H., Li, F., and Jiang, C.: Long-term trend of visibility and its characterizations in the Pearl River Delta (PRD) region, China, Atmos. Environ., 42,

10   1424-1435, doi: 10.1016/j.atmosenv.2007.11.025, 2008.

Fu, C., Wu, J., Gao, Y., Zhao, D., and Han, Z.: Consecutive extreme visibility events in China during 1960–2009, Atmos. Environ., 68, 1-7, doi: 10.1016/j.atmosenv.2012.11.035, 2013.

Gao, L., Jia, G., Zhang, R., Che, H., Fu, C., Wang, T., Zhang, M., Jiang, H., and Yan, P.: Visual range trends in the Yangtze River Delta Region of China, 1981–2005, J. Air Waste Manage. Assoc.,

15   61, 843-849, doi: 10.3155/1047-3289.61.8.843, 2011.

Gysel, M., Crosier, J., Topping, D. O., Whitehead, J. D., Bower, K. N., Cubison, M. J., Williams, P. I., Flynn, M. J., McFiggans, G. B., and Coe, H.: Closure study between chemical composition and hygroscopic growth of aerosol particles during TORCH2, Atmos. Chem. Phys., 7, 6131-6144, doi: 10.5194/acp-7-6131-2007, 2007.

20   Hao, L., Yang, W., Wu, T., Shi, G., Zhao, J., and Tan, Y.: Analysis of radiative properties of BC-sulfate aerosols, Plateau Meteorol., 1238-1245, 2010.

Jimenez, J. L., Canagaratna, M. R., Donahue, N. M., Prevot, A. S. H., Zhang, Q., Kroll, J. H., DeCarlo, P. F., Allan, J. D., Coe, H., Ng, N. L., Aiken, A. C., Docherty, K. S., Ulbrich, I. M., Grieshop, A. P., Robinson, A. L., Duplissy, J., Smith, J. D., Wilson, K. R., Lanz, V. A., Hueglin, C., Sun,

25   Y. L., Tian, J., Laaksonen, A., Raatikainen, T., Rautiainen, J., Vaattovaara, P., Ehn, M., Kulmala, M., Tomlinson, J. M., Collins, D. R., Cubison, M. J., Dunlea, J. E., Huffman, J. A., Onasch, T. B., Alfarra, M. R., Williams, P. I., Bower, K., Kondo, Y., Schneider, J., Drewnick, F., Borrmann, S., Weimer, S., Demerjian, K., Salcedo, D., Cottrell, L., Griffin, R., Takami, A., Miyoshi, T., Hatakeyama, S., Shimono, A., Sun, J. Y., Zhang, Y. M., Dzepina, K., Kimmel, J.

30   R., Sueper, D., Jayne, J. T., Herndon, S. C., Trimborn, A. M., Williams, L. R., Wood, E. C.,

Middlebrook, A. M., Kolb, C. E., Baltensperger, U., and Worsnop, D. R.: Evolution of organic aerosols in the atmosphere, Science, 326, 1525-1529, doi: 10.1126/science.1180353, 2009.

Kang, H., Zhu, B., Su, J., Wang, H., Zhang, Q., and Wang, F.: Analysis of a long-lasting haze episode in Nanjing, China, Atmos. Res., 120, 78-87, 2013.

5   King, S. M., Rosenoern, T., Shilling, J. E., Chen, Q., Wang, Z., Biskos, G., McKinney, K. A., Pöschl, U., and Martin, S. T.: Cloud droplet activation of mixed organic-sulfate particles produced by the photooxidation of isoprene, Atmos. Chem. Phys., 10, 3953-3964, 2010.

Köhler, H.: The nucleus in and the growth of hygroscopic droplets, Trans. Faraday Soc., 32, 1152-1161, 1936.

10   Kreidenweis, S. M., Petters, M. D., and DeMott, P. J.: Single-parameter estimates of aerosol water content, Environ. Res. Lett., 3, 035002, 2008.

Lee, S. C., and Tien, C. L.: Optical constants of soot in hydrocarbon flames, Symposium (International) on Combustion, 18, 1159-1166, 1981.

Lesins, G., Chylek, P., and Lohmann, U.: A study of internal and external mixing scenarios and its

15   effect on aerosol optical properties and direct radiative forcing, J. Geophys. Res. Atmos. (1984–2012), 107, AAC 5-1-AAC 5-12, 2002.

Levoni, C., Cervino, M., Guzzi, R., and Torricella, F.: Atmospheric aerosol optical properties: a database of radiative characteristics for different components and classes, Appl. Optics, 36, 8031-8041, 1997.

20   Lin, Z. J., Tao, J., Chai, F. H., Fan, S. J., Yue, J. H., Zhu, L. H., Ho, K. F., and Zhang, R. J.: Impact of relative humidity and particles number size distribution on aerosol light extinction in the urban area of Guangzhou, Atmos. Chem. Phys., 13, 1115-1128, 2013.

Liu, B. Y. H.: A wide-range particle spectrometer for aerosol measurement from 0.010 μm to 10 μm, Aerosol. Air Qual. Res., 10, 125-139, doi: 10.4209/aaqr.2009.10.0062, 2010.

25   Liu, H. J., Zhao, C. S., Nekat, B., Ma, N., Wiedensohler, A., van Pinxteren, D., Spindler, G., Müller, K., and Herrmann, H.: Aerosol hygroscopicity derived from size-segregated chemical composition and its parameterization in the North China Plain, Atmos. Chem. Phys., 14, 2525-2539, 2014.

Ma, N., Zhao, C. S., Müller, T., Cheng, Y. F., Liu, P. F., Deng, Z. Z., Xu, W. Y., Ran, L., Nekat, B., and

30   Pinxteren, D. v.: A new method to determine the mixing state of light absorbing carbonaceous

using the measured aerosol optical properties and number size distributions, Atmos. Chem. Phys., 12, 2381-2397, 2012.

Mcmurry, P. H.: A review of atmospheric aerosol measurements, Atmos. Environ., 34, 1959-1999, 2000.

5 Miao, Q., Zhang, Z., Li , Y., Duan, Q., Qin, X., and Xu , B.: Size distributions of carbonaceous aerosols and their potential sources at Mt.Huang during Summer., Environ. Sci. Chinese, 35, 1938-1946, 2015.

Petters, M. D., and Kreidenweis, S. M.: A single parameter representation of hygroscopic growth and cloud condensation nucleus activity, Atmos. Chem. Phys., 7, 1961-1971, 2007.

10 Petters, M. D., and Kreidenweis, S. M.: A single parameter representation of hygroscopic growth and cloud condensation nucleus activity – Part 2: Including solubility, Atmos. Chem. Phys., 8, 6273-6279, doi: 10.5194/acp-8-6273-2008, 2008.

Qian, Y., and Giorgi, F.: Regional climatic effects of anthropogenic aerosols? The case of southwestern China, Geophys. Res. Lett., 27, 3521-3524, doi: 10.1029/2000GL011942, 2000.

15 Qian, Y., Wang, W., Leung, L. R., and Kaiser, D. P.: Variability of solar radiation under cloud-free skies in China: The role of aerosols, Geophys. Res. Lett., 34, L12804, doi: 10.1029/2006GL028800, 2007.

Redemann, J., Turco, R. P., Liou, K. N., Russell, P. B., Bergstrom, R. W., Schmid, B., Livingston, J. M., Hobbs, P. V., Hartley, W. S., and Ismail, S.: Retrieving the vertical structure of the effective
20 aerosol complex index of refraction from a combination of aerosol in situ and remote sensing measurements during TARFOX, J. Geophys. Res. Atmos. (1984–2012), 105, 9949-9970, 2000.

Seinfeld, J. H., and Pandis, S. N.: Atmospheric Chemistry and Physics: From Air Pollution to Climate Change, John Wiley & Sons, New York, 2012.

25 Stock, M., Cheng, Y. F., Birmili, W., Massling, A., Wehner, B., Müller, T., Leinert, S., Kalivitis, N., Mihalopoulos, N., and Wiedensohler, A.: Hygroscopic properties of atmospheric aerosol particles over the Eastern Mediterranean: implications for regional direct radiative forcing under clean and polluted conditions, Atmos. Chem. Phys., 11, 4251-4271, 2011.

Streets, D. G., Yu, C., Wu, Y., Chin, M., Zhao, Z., Hayasaka, T., and Shi, G.: Aerosol trends over China,
30 1980－2000 ☆, Atmos. Res., 88, 174–182, 2008.

Atmospheric
Chemistry
and Physics
Discussions

Tang, I. N.: Chemical and size effects of hygroscopic aerosols on light scattering coefficients, J. Geophys. Res., 101, 19,245-219,250, 1996.

Tie, X., Wu, D., and Brasseur, G.: Lung cancer mortality and exposure to atmospheric aerosol particles in Guangzhou, China, Atmos. Environ., 43, 2375-2377, 2009.

5   Topping, D. O., McFiggans, G. B., and Coe, H.: A curved multi-component aerosol hygroscopicity model framework: Part 1 – Inorganic compounds, Atmos. Chem. Phys., 5, 1205-1222, doi: 10.5194/acp-5-1205-2005, 2005.

Watson, J. G.: Visibility: Science and regulation, J. Air Waste Manage. Assoc., 52, 628-713, doi: 10.1080/10473289.2002.10470813, 2002.

10   Wehner, B., Birmili, W., Ditas, F., Wu, Z., Hu, M., Liu, X., Mao, J., Sugimoto, N., and Wiedensohler, A.: Relationships between submicrometer particulate air pollution and air mass history in Beijing, China, 2004–2006, Atmos. Chem. Phys., 8, 6155-6168, 2008.

Wen, C.-C., and Yeh, H.-H.: Comparative influences of airborne pollutants and meteorological parameters on atmospheric visibility and turbidity, Atmos. Res., 96, 496-509, 2010.

15   Wex, H., Neusüß, C., Wendisch, M., Stratmann, F., Koziar, C., Keil, A., Wiedensohler, A., and Ebert, M.: Particle scattering, backscattering, and absorption coefficients: An in situ closure and sensitivity study, J. Geophys. Res. Atmos. (1984–2012), 107, LAC 4-1-LAC 4-18, 2002.

Wright, H. L.: Atmospheric opacity at valentia, Q. J. R. Meteorol. Soc., 66, 209–213, 1940.

Wu, D., Tie, X., Li, C., Ying, Z., Lau, A. K.-H., Huang, J., Deng, X., and Bi, X.: An extremely low
20   visibility event over the Guangzhou region: A case study, Atmos. Environ., 39, 6568-6577, 2005.

Yu, X., Ma, J., Zhu, B., Wang, H., Yan, S., and Xia, H.: Effects of relative humidity and aerosol physicochemical properties on atmospheric visibility in northern suburb of Nanjing, Environ. Sci., 36, 1919-1925, 2015.

25   Zhang, X., and Mcmurry, P. H.: Evaporative losses of fine particulate nitrates during sampling, Atmos. Environ., 26, 3305–3312, 1992.

Zhang, Y., Zhang, P., Wang, J., Qu, E., Liu, Q., and Li, G.: Climatic characteristics of persistent haze events over Jingjinji during 1981-2013, Meteorol. Mon., 311-318, 2015.

Zou, J., An, J., Wang, H., Shao, P., Duan , Q., Xue , G., and Pang , B.: Distribution characteristics of
30   pollution gases and water soluble ion in aerosol during the Asian youth games of Nanjing,

China, Environ. Sci., 35, 4044-4051, 2014.
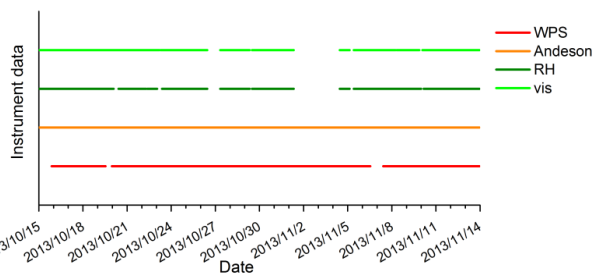
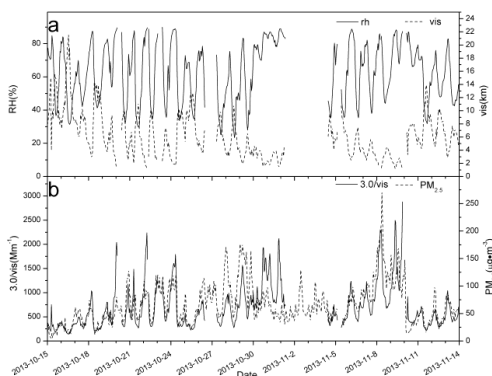5   Fig. 1 Missing data from instruments during the observation period

Fig. 2 Time series of RH, visibility, extinction coefficient, and PM$_{2.5}$ during the observation
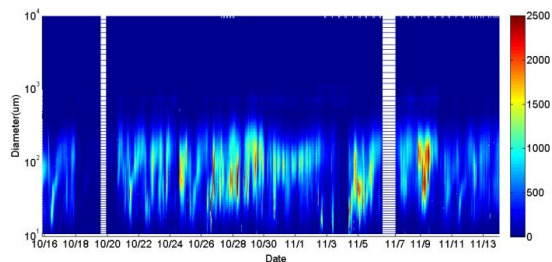

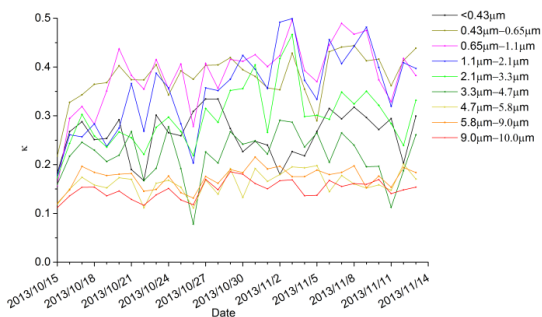Fig. 3 Time series of size distribution (dry particles) during the observation period

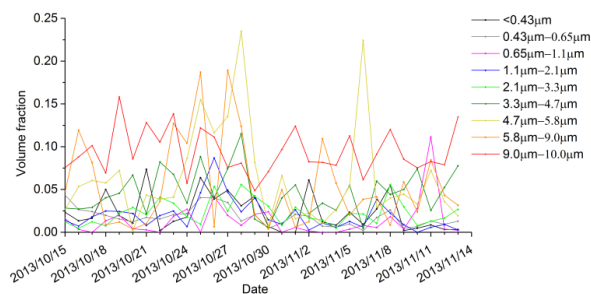Fig. 4 Time series of κ in different sizes during the observation period

Fig. 5 Time series of the volume fraction of EC in different size segments during the observation period
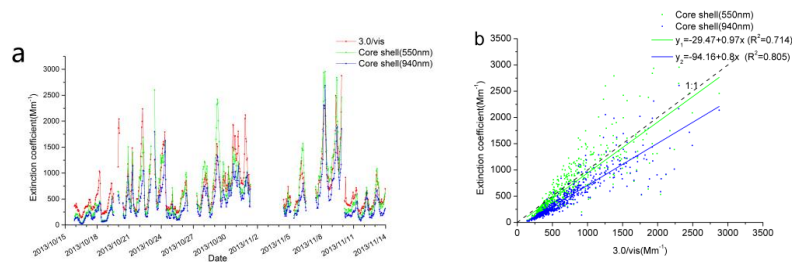
Fig. 6 Relativities of calculated and observed values by the core-shell model (λ=550 nm, 940 nm)
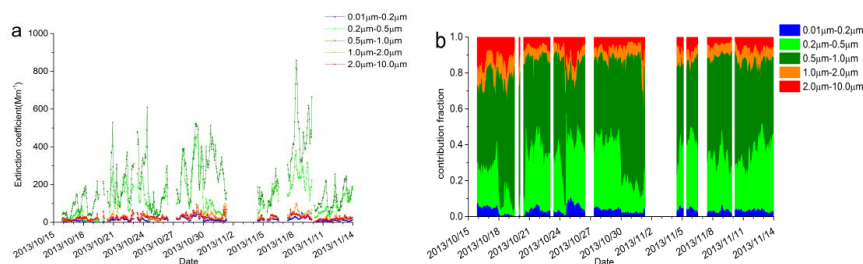

Fig. 7 Time series of extinction coefficients (a) and the contribution fraction of extinction coefficients (b) in different

size segments under dry conditions

Atmospheric
Chemistry
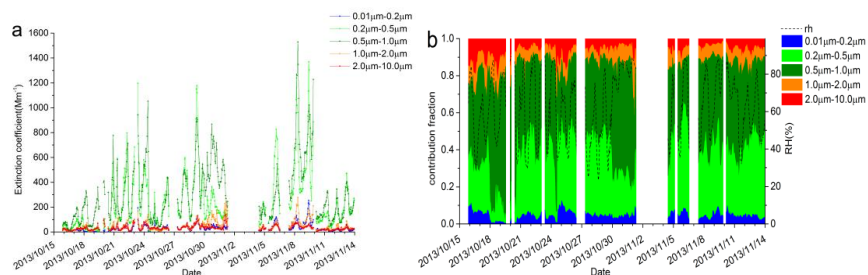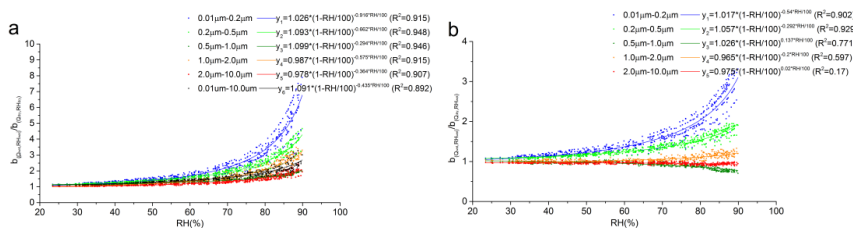and Physics
Discussions

Fig. 8 Time series of extinction coefficients (a) and the contribution fraction of extinction coefficients (b) in different size segments at ambient relative humidity

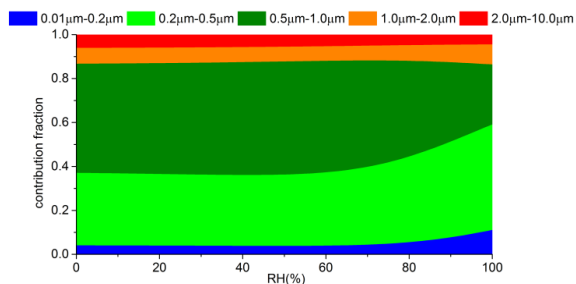5   Fig. 9 The effect of relative humidity on extinction

Fig. 10 Relationship between the contribution fraction of extinction coefficients in different size segments and relative humidity (RH)

10   Table 1 Properties of each pure material

	Molecular weight	Density (g cm^{-3})	κ
NH$_4$NO$_3$	80.04	1.72	0.68
H$_2$SO$_4$	98.08	1.83	1.13
NH$_4$HSO$_4$	115.11	1.78	0.56
(NH$_4$)$_2$SO$_4$	132.14	1.77	0.53
WSOC		1.40	0.10

Table 2 Input/output parameters of efficiency factor (Q)

Atmospheric
Chemistry
and Physics
Discussions

Open Access
EGU

input parameters	output parameters
$X_{cor} = \dfrac{\pi \cdot \sqrt[3]{\frac{V_{EC}}{V_{tol}}} \times D_0}{\lambda}$	
	Q_{ext}
$X_{man} = \dfrac{\pi \cdot D_0 \cdot GF}{\lambda}$	ω_0
$m_{cor} = (1.8, 0.54)$	
$m_{man} = (\dfrac{1.53 + 1.33(GF-1)^3}{(GF-1)^3 + 1}, 0)$	